Influence of the parallel nonlinearity on zonal flows and heat transport in global gyrokinetic particle-in-cell simulations

S. Jolliet,[1] B. F. McMillan,[1] T. Vernay,[1] L. Villard,[1] R. Hatzky,[2] A. Bottino,[3] and P. Angelino[4]

[1]*Ecole Polytechnique Fédérale de Lausanne (EPFL), Centre de Recherches en Physique des Plasmas, Association Euratom-Confédération Suisse, CH-1015 Lausanne, Switzerland*
[2]*Rechenzentrum der Max-Planck-Gesellschaft und des Max-Planck-Institutes für Plasmaphysik, EURATOM-Association, D-85748 Garching, Germany*
[3]*Max-Planck-Institut für Plasmaphysik, Boltzmannstr. 2, D-85748 Garching, Germany*
[4]*Association Euratom CEA, CEA/DSM/IRFM, Cadarache, 13108 Saint-Paul-lez-Durance, France*

In this paper, the influence of the parallel nonlinearity on zonal flows and heat transport in global particle-in-cell ion-temperature-gradient simulations is studied. Although this term is in theory orders of magnitude smaller than the others, several authors [L. Villard, P. Angelino, A. Bottino *et al.*, Plasma Phys. Contr. Fusion **46**, B51 (2004); L. Villard, S. J. Allfrey, A. Bottino *et al.*, Nucl. Fusion **44**, 172 (2004); J. C. Kniep, J. N. G. Leboeuf, and V. C. Decyck, Comput. Phys. Commun. **164**, 98 (2004); J. Candy, R. E. Waltz, S. E. Parker *et al.*, Phys. Plasmas **13**, 074501 (2006)] found different results on its role. The study is performed using the global gyrokinetic particle-in-cell codes TORB (theta-pinch) [R. Hatzky, T. M. Tran, A. Könies *et al.*, Phys. Plasmas **9**, 898 (2002)] and ORB5 (tokamak geometry) [S. Jolliet, A. Bottino, P. Angelino *et al.*, Comput. Phys. Commun. **177**, 409 (2007)]. In particular, it is demonstrated that the parallel nonlinearity, while important for energy conservation, affects the zonal electric field only if the simulation is noise dominated. When a proper convergence is reached, the influence of parallel nonlinearity on the zonal electric field, if any, is shown to be small for both the cases of decaying and driven turbulence. © *2009 American Institute of Physics*. [DOI: 10.1063/1.3174433]

I. INTRODUCTION

Microturbulence is believed to be responsible for anomalous transport measured in tokamaks.[1] Anomalous transport is best described with the gyrokinetic theory and in particular with gyrokinetic codes. Independent of how complex the physical model is, the reliability of such codes relies mainly on two points: the analytical model used to derive the gyrokinetic equation and the numerical properties of the simulation. The latter point is usually checked with code benchmarks, such as the CYCLONE test case[2] and is a crucial stage to validate a numerical code. The pioneering works on the gyrokinetic equation in a general magnetic configuration were carried by Taylor and Hastie[3] and by Rutherford and Frieman[4] using an eikonal representation and describing linear effects only. Then a nonlinear gyrokinetic equation was obtained by Frieman and Chen[5] by first introducing the magnetic coordinates and then averaging the Vlasov equation over the gyroangle. All these approaches are not suitable for particle simulations. The next important step has been done by Lee,[6] unfortunately until that time all these models had the disadvantage that the original energy conservation was broken. Therefore, a more elegant Hamiltonian approach was used by Dubin *et al.*[7] for the electrostatic case in slab geometry. The more general action-variational method, which also starts from a Hamiltonian, has been first developed by Littlejohn[8] in general geometry and further applied by Hahm[9] to the electrostatic case. This technique has then been extended to further physical effects such as equilibrium flow,[10] electromagnetic perturbations,[11] and the bounce-averaged gyrokinetic equation.[12] Besides having an energy invariant (leading to the denomination of "first principles" simulations), this technique introduces a new nonlinear term in the equations of motion, namely, the *parallel nonlinearity*, or $v_{\parallel}$-nonlinearity (VNL). This term, representing the nonlinear Landau damping, is usually neglected because it is one order smaller than the other terms, although it formally appears on the action-variational method. Despite this theoretical argument, it has been observed that the role of the VNL is controversial. In Ref. 13, flux-tube Eulerian and particle-in-cell (PIC) simulations revealed no influence of the VNL in tokamak geometry, while global PIC simulations using the ORB5 (Ref. 14) code found an influence on the zonal flow structure and simulations using the UCAN code[15] found an influence on the saturation level and on the heat flux. In theta-pinch geometry, the global PIC code TORB (Ref. 16) found that the zonal flow profile is affected by the VNL, while the global PIC code G3D and the global Eulerian code G4D found no effect (see Ref. 17).

In this work, the role of the VNL is revisited using the global, electrostatic, collisionless PIC codes TORB (Ref. 18) and ORB5.[19] Compared to the version used in Ref. 14, many improvements have been brought to ORB5, in particular, a field-aligned Fourier technique,[19] a signal to noise ratio diagnostic,[20] and a noise-control algorithm.[21] Therefore, new CYCLONE simulations have been carried out with more confidence on the results. In particular, the possibility that the numerical noise and the influence of the VNL are

16, 072309-1

linked is explored for the two cases of decaying and driven turbulence.

The remainder of the paper is organized as follows. In Sec. II, the theoretical expression of the VNL is discussed and the ORB5 code is briefly described. In Sec. III, simulation results for decaying turbulence are shown, while the driven turbulence case is presented in Sec. IV and the conclusions are exposed in Sec. V.

II. GYROKINETIC MODEL AND DEFINITION OF PARALLEL NONLINEARITY

The gyrokinetic model used throughout this work is the standard electrostatic collisionless model with adiabatic electrons, used to study ion-temperature-gradient (ITG) turbulence. It is described in more details in Ref. 19, but the important points for the reader are briefly described below. The code is global, i.e., profiles evolve self-consistently. The gyrokinetic equation is the one from Hahm.[9] In particular, the following gyrokinetic ordering is used:

$$\frac{\omega}{\Omega_i} \sim \frac{k_\parallel}{k_\perp} \sim \frac{e\phi}{T_e} \sim \frac{\rho_{Li}}{L_n} \sim \frac{\rho_{Li}}{L_{Ti}} \sim \frac{\rho_{Li}}{L_{Te}} \sim \mathcal{O}(\epsilon_g), \tag{1}$$

$$\frac{\rho_{Li}}{L_B} \sim \mathcal{O}(\epsilon_B), \quad k_\perp \rho_{Li} \sim \mathcal{O}(1), \tag{2}$$

where ω is the characteristic fluctuation frequency, $\Omega_i = q_i B_0 / m_i$ is the ion cyclotron frequency, q_i is the ion charge, B_0 is the magnetic field at axis, m_i is the ion mass, $k_\parallel$ and $k_\perp$ are the parallel and perpendicular components of the wave vector with respect to the magnetic field, ϕ is the fluctuating electrostatic potential, ρ_{Li} is the ion gyroradius, and L_n, L_{Ti}, L_{Te}, L_B are the characteristic lengths associated with density, ion temperature, electron temperature, and magnetic field profiles. ϵ_g and ϵ_B are small parameters, $\epsilon_g \sim \rho^*$, $\epsilon_B \sim \epsilon_a \epsilon_g$, with $\rho^* = \rho_s / a \ll 1$, ρ_s is the ion sound gyroradius, a is the minor radius of the tokamak, and ϵ_a is the inverse aspect ratio. The equations of motion are

$$\frac{d\vec{R}}{dt} = v_\parallel \vec{h} + \frac{1}{\Omega_i B_\parallel^*} \left(v_\parallel^2 + \frac{v_\perp^2}{2} \right) (\vec{h} \times \nabla B)$$

$$- \frac{v_\parallel^2}{\Omega_i B_\parallel^*} \vec{h} \times [\vec{h} \times (\nabla \times \vec{B})] + \frac{\langle \vec{E} \rangle \times \vec{B}}{B_\parallel^* B}, \tag{3}$$

$$\frac{dv_\parallel}{dt} = \frac{1}{2} v_\perp^2 \nabla \cdot \vec{h} + \frac{v_\perp^2 v_\parallel}{2 B_\parallel^* \Omega_i B} \{\vec{h} \times [\vec{h} \times (\nabla \times B)]\} \cdot \nabla B$$

$$+ \text{VNL}, \tag{4}$$

and the last one states that the magnetic moment per mass unit $\mu = v_\perp^2 / (2B)$ is conserved. $\vec{R}$ is the guiding center coordinate vector, $\vec{h} = \vec{B}/B$, $v_\parallel$ (respectively, $v_\perp$) are the velocities parallel (respectively, perpendicular) to the magnetic field, $B_\parallel^* = B + B v_\parallel / \Omega_i (\nabla \times \vec{h}) \cdot \vec{h}$, and $\langle \vec{E} \rangle$ is the gyroaveraged

electric field. The nonlinear component of the last equation is called the $v_\parallel$-nonlinearity and is

$$\text{VNL} = \underbrace{\frac{q_i}{m_i} E_\parallel}_{\mathcal{O}(\epsilon_g^2)} + \underbrace{\frac{v_\parallel}{BB^*} \langle \vec{E} \rangle \cdot (\vec{h} \times \nabla B)}_{\mathcal{O}(\epsilon_g \epsilon_B)}$$

$$- \underbrace{\frac{v_\parallel}{BB_\parallel^*} \langle \vec{E} \rangle \cdot \{\vec{h} \times [\vec{h} \times (\nabla \times B)]\}}_{\mathcal{O}(\epsilon_g \epsilon_B)}. \tag{5}$$

The first term of the VNL is proportional to the parallel electric field, insensitive to zonal flows and of order ϵ_g^2. While in decaying ITG simulations the system rapidly becomes dominated by the zonal flow, which suppresses turbulence, the turbulent modes $n \neq 0$ have a much stronger activity in driven ITG simulations. The resulting higher parallel electric field may yield a stronger influence of the VNL as compared to the decaying case.[17] The second and third terms are due to magnetic curvature, sensitive to zonal flows, and of order $\epsilon_g \epsilon_B$, i.e., roughly smaller by ϵ_a^{-1} than the first term. All the other terms in the equations of motion are of the order of 1, ϵ_B or ϵ_g, i.e., much larger than the VNL.

The distribution function f is decomposed into an equilibrium Maxwellian $f_0(\hat{\psi}, \epsilon, \mu)$ and a perturbed part $\delta f(\vec{z}, t)$, where $\hat{\psi}$, ϵ, and μ are constants of the unperturbed motion. $\hat{\psi}$ is a constant of motion derived from the canonical angular momentum to avoid the generation of spurious zonal flows,[22] ϵ is the kinetic energy per mass unit, and $\vec{z} = (\vec{R}, v_\parallel, \mu)$. The Vlasov equation reads

$$\frac{d\delta f}{dt} = \tau(\vec{E}) + S_K(\vec{z}, t) + S_{\text{corr}}(\vec{z}, t), \tag{6}$$

$$\tau(\vec{E}) = -f_0 \kappa(\hat{\psi}) \left. \frac{d\hat{\psi}}{dt} \right|_1 + \frac{q_i f_0}{T_i} \langle \vec{E} \rangle \cdot \left. \frac{d\vec{R}}{dt} \right|_0, \tag{7}$$

where $\tau(\vec{E})$ is the collisionless right hand side of the Vlasov equation. The subscript 0 (respectively, 1) denotes the unperturbed (respectively, perturbed) motion, $\kappa(\hat{\psi}) = \partial \ln f_0 / \partial \hat{\psi}$ and T_i is the ion temperature. $S_K(\vec{z}, t) = -\gamma_K \delta f(\vec{z}, t)$ is the Krook operator, where γ_K is the Krook damping coefficient and defines the amplitude of the artificial dissipation and is specified on input. The Krook operator is further modified with the operator $S_{\text{corr}}(\vec{z}, t)$, which can be tuned such that the Krook operator does not modify a given set of moments. In particular, S_{corr} can be cast in such a way that the Krook operator does not introduce thermal energy into the system. In this case, the turbulence will be decaying, like for the usual collisionless cases without dissipation. In the opposite case, the temperature profile will not relax and the turbulence will be driven. More details on the Krook operator can be found in Ref. 21. In its current state, the Krook operator does not conserve parallel momentum, although this modification would be easy to implement. The consequences will be briefly discussed in Sec. IV. Note that a recent version of ORB5 using the noise-control algorithm has been bench-

marked nonlinearly against other gyrokinetic codes for the CYCLONE test case.[23] An important remark on the Vlasov equation is that formally ORB5 is not a δf code: the decomposition employed can be viewed as a "control variate" technique,[24] which is a numerical artifact and has no real physical meaning. f_0 is arbitrary, but its choice will of course affect the numerical noise in the simulation. When the Krook operator is turned off, the Vlasov equation expresses the conservation of f. Formally, the Vlasov equation is, in this case,

$$-\frac{df_0}{dt} = \left.\frac{d\delta f}{dt}\right|_0 + \left.\frac{\partial \delta f}{\partial t}\right|_1 + \nabla \delta f \cdot \left.\frac{d\vec{R}}{dt}\right|_1 + \underbrace{\left.\frac{\partial \delta f}{\partial v_\parallel}\frac{dv_\parallel}{dt}\right|_1}_{\equiv \text{VNL}}. \quad (8)$$

Therefore f is no longer conserved if the VNL is omitted in the equations of motion.

The system can be initialized in several ways: in the *random initialization*, the weight of the markers describing δf is given a random initial value using Hammersley sequences.[25] In the *mode initialization*, the initial perturbation is given by a superposition of cosine perturbations, i.e., $\delta f(t_0) \propto \sum_{m=m_1}^{m_2} \sum_{n=n_1}^{n_2} \cos(m\theta_* - n\varphi)$, where m_1, m_2, n_1, and n_2 are input parameters, θ_* and φ are the straight-field-line and toroidal angles of the markers, and m and n are the poloidal and toroidal wave numbers.

When the Krook operator is turned off, a global energy invariant can be analytically derived,[18]

$$E(t_0) = \int \frac{1}{2}m_i v^2 f(\vec{z},t)\mathrm{d}\vec{z} + \frac{q_i}{2}\int \mathrm{d}\vec{x}\,\phi(\vec{x},t)\,\delta n_i(\vec{x},t), \quad (9)$$

where $E(t_0) = E(t) = E_k(t) + E_f(t)$ is the total energy of the system, $E_k(t)$ is the total kinetic energy of the system, $E_f(t)$ is the total field energy of the system, $\phi(\vec{x})$ is the electrostatic potential, and $\delta n_i(\vec{x})$ is the perturbed density. In particular, the temporal relative energy conservation $\Delta E/E_f(t)$ can be computed, where $\Delta E = E(t) - E(t_0)$. In the beginning of the simulation, this quantity that can be quite large as $E_f(t)$ is extremely small, but in the nonlinear phase this expression is meaningful and is a good indicator of the quality of the simulation. Due to the Monte Carlo approach, PIC simulations suffer from statistical noise. It is generally observed that the energy conservation degrades in the nonlinear phase, which can impair the quality of the simulation. This invariant is no longer valid when the VNL is not retained in the equations of motion. Besides the noise-control algorithm described above, the particularity of ORB5 is the field-aligned Fourier filtering technique.[19] By suppressing modes that do not satisfy the gyrokinetic ordering Eq. (1), a massive improvement of the energy conservation is obtained and the signal to noise ratio[20] is improved by a factor of ρ_*^{-1}. The important parameter for the noise study is the number of markers per Fourier modes and not the number of markers per grid cell.[20]

The gyrokinetic model of TORB is described in Ref. 18. It is basically the same model than in ORB5 except that the geometry is a theta-pinch (see Ref. 16 for the expression of
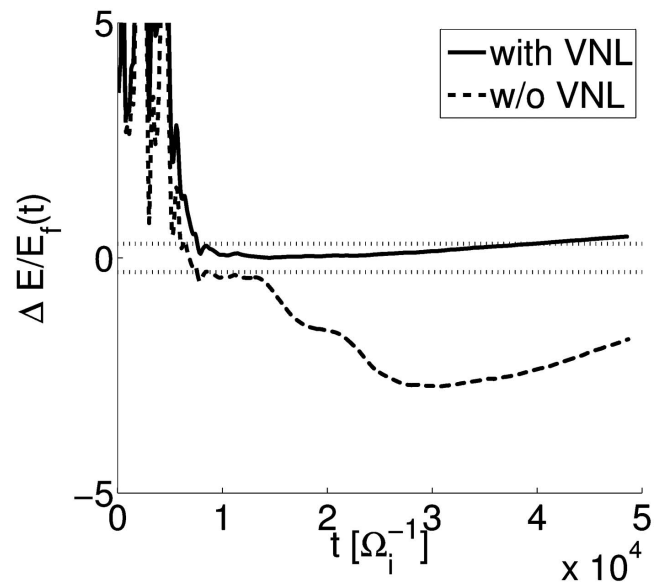

FIG. 1. Relative energy conservation as a function of time for the TORB simulation with (solid line) and without (dashed line) the VNL. The dotted lines represent a relative energy conservation of $\pm 30\%$.

the magnetic field). TORB does not have a Krook operator but an optimized loading technique is implemented and described in Ref. 18.

III. SIMULATION RESULTS FOR DECAYING TURBULENCE

A. TORB simulations

The TORB code has been run using the parameters from Ref. 18: $\rho^* = 1/135$, $L_z = 8456\rho_{Li}$, and $L_n = \infty$. The quasineutrality equation is solved on a $N_s = 64$, $N_\theta = 256$, and $N_z = 32$ grid and a rectangular Fourier filter $-6 \le n \le 6$, $-96 \le m \le 96$ is used. The number of markers is $2^{27} \cong 134$ m, which corresponds to 256 markers per cell and 1670 markers per Fourier mode. The time step is $\Delta t = 100\ \Omega_i^{-1}$ in the linear phase and $\Delta t = 30\ \Omega_i^{-1}$ in the nonlinear phase. Two simulations have been performed, one with and the other without the VNL. The difference between these simulations and the simulations from Ref. 16 is that the optimized loading used here is a smoother one (details are given below).

Figure 1 shows the temporal evolution of the relative energy conservation $\Delta E/E_f(t)$. One sees that the case with VNL has a satisfactory energy conservation ($\sim 30\%$) up to $t \sim 4 \times 10^4\ \Omega_i^{-1}$, but the accumulation of the noise degrades the energy conservation. On the other hand, the simulation without the VNL does not have energy conservation as expected. Next, the radial profile of the zonal electric field $\nabla \bar{\phi}$, where the bar denotes the flux-surface-averaged potential, is displayed in the late nonlinear phase on Fig. 2. From this figure it is clear that the VNL does not play any role. It contradicts previous TORB simulations published in Ref. 16, in which two examples are shown of how numerical sampling noise can lead to an erroneous zonal flow pattern. Figure 1 of that paper shows how an improved loading procedure is applied successfully in order to preserve the long
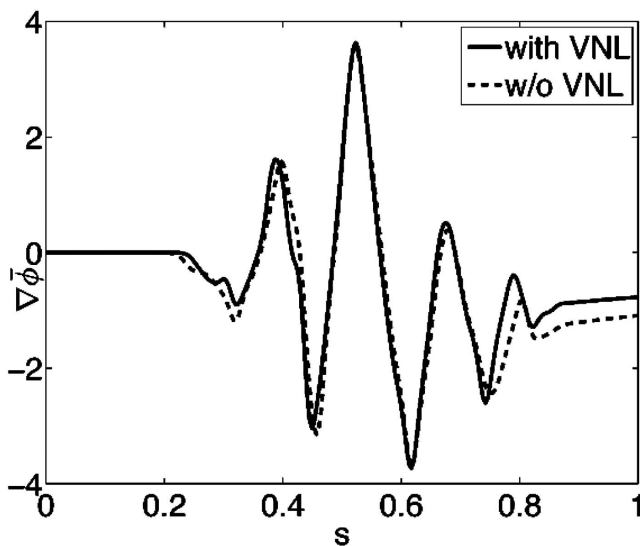
FIG. 2. Profile of the radial electric field at the end of the simulation for the TORB simulation with (solid line) and without (dashed line) the VNL.

FIG. 3. Temporal evolution of the radial heat flux for the TORB simulation with (solid line) and without (dashed line) the VNL.

term zonal flow structure. This procedure consists in performing successive simulations in which the distribution of markers of the next simulation is constructed from the distribution of marker weights absolute values of the previous simulation at a given time t_{NL}. For the case shown there the radial structure of the resulting marker distribution resembles that of the zonal flows; in some radial regions there are a lot of markers and in others hardly any. Such a distribution would be a good choice if the zonal flow structure during the whole nonlinear period of the optimized-loading simulation was similar to that in the nonoptimized-loading simulation at t_{NL}. However, this is clearly not the case (as shown in Fig. 1 of that paper) and the "optimized" loading procedure can go astray, as is the case for the run without VNL show in Fig. 3 of that paper, in which the effect on the zonal flow structure was erroneously ascribed to the absence of VNL. After having revisited these simulations for the present paper, we now attribute it to the effect of numerical sampling noise. In the present paper, such problem is avoided by employing a radially smoothed optimized loading, for example, fitted with a broad Gaussian, as originally suggested in Ref. 18. The latter solution has been used in this work and shows that, if not properly applied, the optimized loading can lead to erroneous conclusions. Finally, Fig. 3 shows the temporal evolution of the volume-averaged radial heat flux for both simulations. Unsurprisingly, both curves are very similar. Due to the prominent role of the zonal flows on the heat flux, similar zonal flow profiles should not affect the corresponding fluxes. The results presented here confirm the theoretical picture that the VNL should not influence the simulation.

B. ORB5 transient simulations

In this section, ORB5 *transient* simulations with and without the VNL are presented. The term *transient* refers here to standard collisionless simulations with no Krook operator. Due to the absence of sources, the profiles decay and the fluxes decrease. Unfortunately these simulations can only
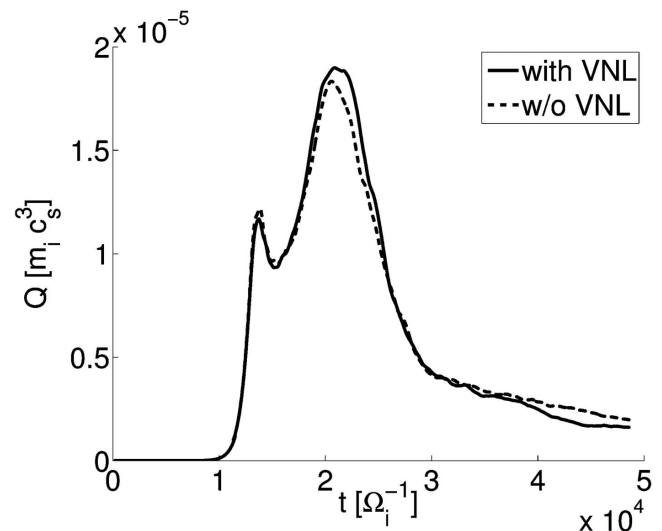
reach a quasisteady state where low order moments are saturated but the sum of the weights squared increases linearly with time.[26] The noise in these simulations can be quite high even at a high number of markers, as will be shown later. The parameters are those from the CYCLONE test case[2] at $\rho^* = 1/184.7$. The physical parameters are $a = 0.625$ m, $B_0 = 1.91$ T, $R_0 = 1.70$ m, $\tilde{\rho}_0 = 0.5$, $q(\tilde{\rho}_0) = 1.4$, $T_i = T_e$, $R_0/L_{Ti} = 6.9$, $\eta_i = L_n/L_{Ti} = 3.12$, and $\hat{s} = 0.78$. B_0 is the magnetic field at axis, R_0 is the major radius, $\tilde{\rho}_0$ is the reference radius in the plasma, q is the safety factor, and $\hat{s}$ is the magnetic shear. A circular equilibrium is used with a safety factor profile given by $q(\tilde{\rho}) = q_0 + (q_{edge} - q_0)\tilde{\rho}^2$, where $\tilde{\rho} = \rho/a$, ρ is the radial coordinate, $q_0 = 0.85$, and $q_{edge} = 3.04$. Numerical parameters are $N = 80 \times 10^6$ markers, $\Delta t = 40$ Ω_i^{-1}. The quasineutrality equation is solved with cubic B-splines on a $N_s = 128$, $N_{\theta_*} = 512$, $N_\varphi = 256$ grid and a field-aligned filtering is applied with $\Delta m = 5$. The latter is combined with a rectangular filter $-57 \le n \le 57$, $128 \le m \le 128$. Poloidal modes above $k_\theta \rho_{Li} = 1.0$ are filtered out. It is known[27] that coupling of short wavelength modes can generate zonal flows. Linearly, ITG modes above $k_\theta \rho_{Li} \cong = 0.8$ are stabilized due to finite Larmor radius effects but they can be nonlinearly generated. These complex nonlinear couplings involve the derivatives of δf and ϕ in all the spatial directions. Numerically, it must therefore be verified that the filtering procedure does not suppress physically important modes. This is done by enlarging the filter until numerical results do not depend on the filter width. In practice, increasing $k_\theta \rho_{Li}$ can modify the local details of the zonal flow profile, but do not modify the radially averaged profiles. Moreover, the quasineutrality equation is valid for $k_\perp \rho_{Li} \sim k_\theta \rho_{Li} \ll 1$, meaning that the response for high $k_\theta \rho_{Li}$ might be incorrect.

Finally, note that 80 m markers correspond to ~5 markers per cell but correspond to ~700 markers per Fourier mode. The temperature profile is shown on Fig. 4.

For transient simulations, the energy invariant is, like for TORB simulations, not valid anymore when the VNL term is dropped out. This can be seen on Fig. 5. The case with the
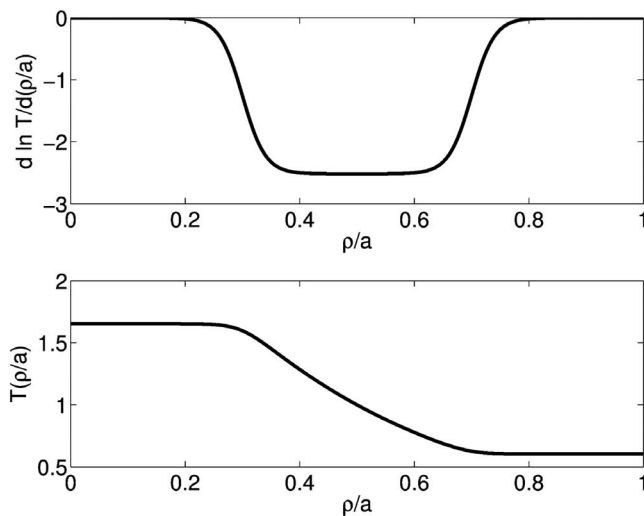
FIG. 4. Logarithmic temperature gradient and temperature profiles used in all the simulations.

FIG. 6. (Color online) Signal to noise ratio for transient simulations with 80 m and 320 m markers, with and without the VNL.

VNL has a relative conservation of energy of about 30% up to $t = 4.6 \times 10^4 \ \Omega_i^{-1}$, which is a good value for a transient PIC simulation. After this time, the relative energy conservation degrades linearly. It is interesting to note that this curve starts to rise at the time where the signal to noise ratio falls below 10 (Fig. 6). It has been found by looking at ITG simulations that convergence was not reached when the signal to noise ratio drops below this value.[21] Figure 5 also reveals that the relative energy conservation is completely lost when the VNL is not included, even if this term is of order ρ_* smaller than the others. This shows the importance of deriving analytically a conservation theorem without any approximation in order to check the correct implementation of the model and the quality of a simulation. It also means that although it has a negligible effect on transport, the VNL should be preferentially kept in transient simulations for numerical reasons.

Next, the influence of the VNL on the zonal flow profiles is examined. Figure 7 shows the profile of the time-averaged radial electric field, time-averaged for the end of the nonlinear phase, for transient simulations with 80 and 320 m, with and without the VNL. When 80 m markers are used, the values at the edge are of different signs and $\nabla \bar{\phi}$ is peaked at midradius for the case without the VNL. From these curves, it could be concluded that the VNL has a strong influence on the zonal flow structures. However, the corresponding profiles for transient simulations with 320 m markers look much more similar. Therefore, one could suspect that the previous observations on the VNL exposed in Ref. 14 have no physical origin but are in fact due to numerical noise, even if the signal to noise ratio looks the same for all the simulations. In fact, this quantity loses his meaning when it approaches unity. This is because the signal and the noise correspond to
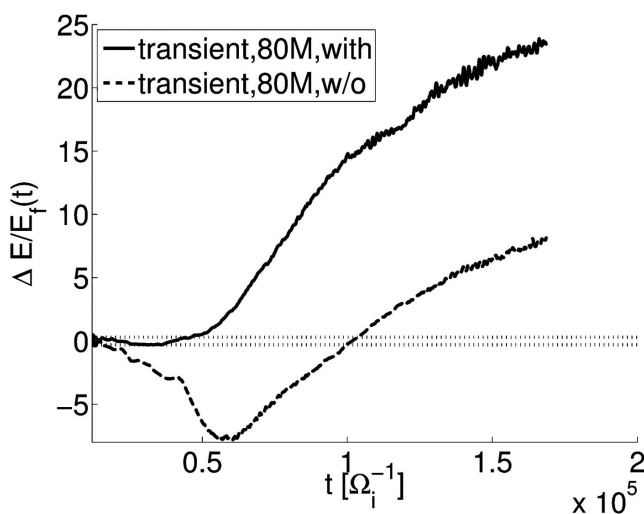

FIG. 5. Relative energy conservation as a function of time for the *transient* simulation with (solid line) and without (dashed line) the VNL. The dotted lines represent a relative energy conservation of ±30%.
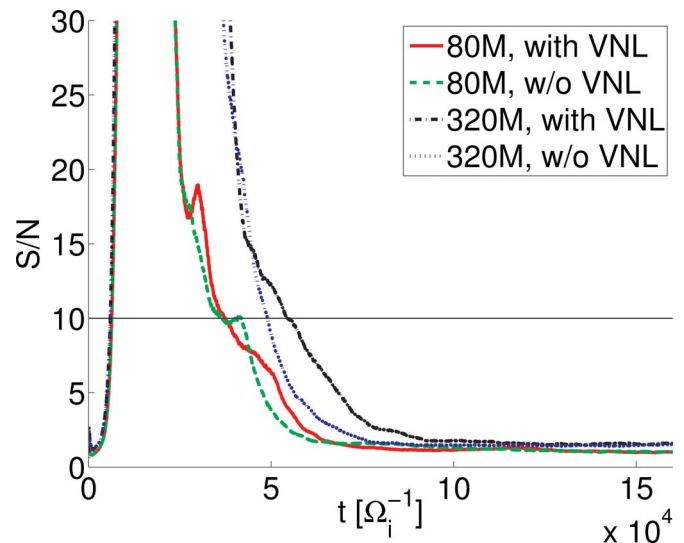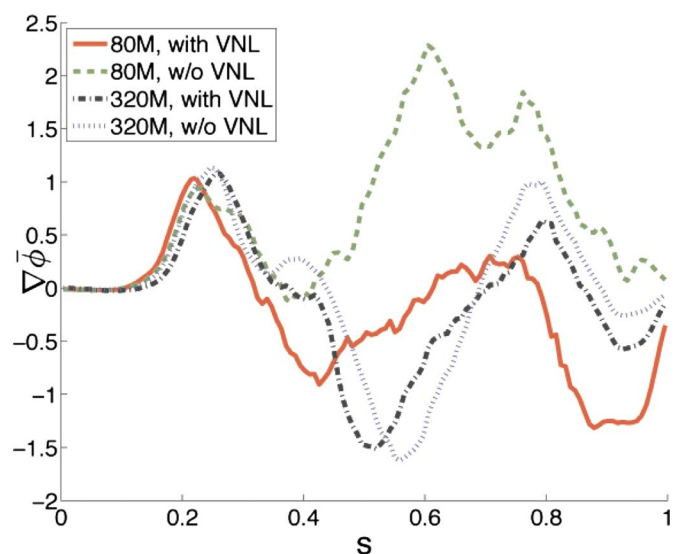

FIG. 7. (Color online) Profile of the radial electric field for transient simulations with 80 and 320 m markers, with and without the VNL. All profiles are time averaged between $t = 10^5$ and $t = 1.5 \times 10^5 \ \Omega_i^{-1}$.
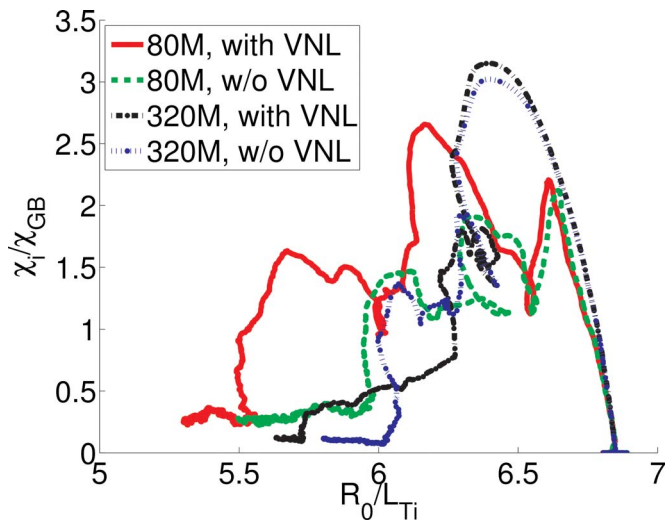
FIG. 8. (Color online) χ_i/χ_{GB} as a function of R_0/L_{Ti} (both profiles are radially averaged between $\tilde{\rho}=0.4$ and $\tilde{\rho}=0.6$) for transient simulations with 80 and 320 m markers, with and without the VNL.
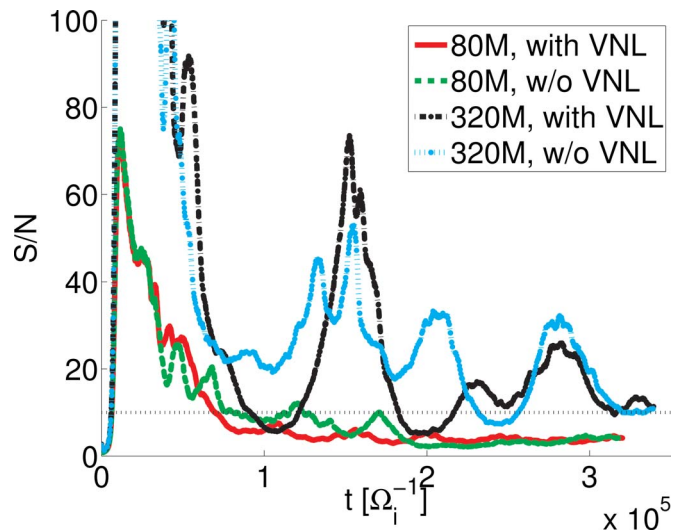
FIG. 9. (Color online) Signal to noise ratio for *noise-controlled* simulations with 80 and 320 m markers, with and without the VNL. The horizontal dotted line indicates a signal to noise ratio of 10.

the perturbed density (in Fourier space) squared for sets of modes inside and outside the field-aligned filter.[20] In particular it is impossible to compute the noisy component of the signal, hence this procedure is not valid anymore when the signal and the noise become comparable. This is what happens in these simulations, where the signal to noise ratio is around 1.5. Therefore one can say that at the end of the nonlinear phase all the simulations are extremely noisy albeit the noise cannot be quantified. Nevertheless, for the 320 m case, the VNL does not seem to play a role on the zonal flow structure. By simply increasing the number of markers, the effect of the VNL almost vanishes. It is therefore likely that numerical effects (noise) overwhelm a possible physical effect of the VNL. It is also evidence that the simulations in Ref. 14 were completely noise dominated. Although the old ORB5 simulations did not have the signal to noise diagnostic, an estimation can be given. According to Ref. 20, the noise scales like

$$\delta n_{i,\text{noise}}^2 \sim \frac{N_m}{N}\langle w^2\rangle G, \qquad (10)$$

where N_m is the number of unfiltered Fourier modes in the simulation, $\langle w^2\rangle$ is the sum of the weights squared and G is some constant depending on the algorithm employed to solve the quasineutrality equation. When going from a square to a field-aligned filter, N_m is reduced by $(\rho^*)^{-1}\sim 200$ and when using the optimized loading, $\langle w^2\rangle$ is reduced by a factor of ~ 5 in the late nonlinear phase.[28] In the old ORB5 simulations, there were approximatively 500 markers per Fourier mode, while there are 700 for the 80 m transient simulations presented here. For all these reasons, it is obvious that for the old ORB5 simulations the optimized loading could not compensate the rectangular filter and consequently the simulations were noise dominated. It is therefore plausible that the observed effects of the VNL in Ref. 14 were in fact a manifestation of numerical noise.

Finally, the effects of the VNL on heat transport in transient simulations are shown on Fig. 8, by looking at χ_i/χ_{GB} as a function of R_0/L_{Ti} during the simulation, where χ_i is the ion heat diffusivity and $\chi_{GB}=(\rho^*)^2 c_s/a$ is the gyro-Bohm normalization. At the end of all the simulations the temperature profile flattens while the heat diffusivity stays constant when both 80 and 320 m are used. This is a clear sign of noise-dominated simulations. Thus, the 320 m transient simulation is unaffected by the VNL but is drowned into noise. Therefore it is desirable to look at the effects of the VNL for noise-reduced simulations by activating the noise-control algorithm.

Note that in Ref. 29 the question of the influence of parallel nonlinearity has been examined. However, those simulations had no sources and used a number of particles per mode of about 20, which is, according to the results presented here, well short of what is necessary. Moreover, it is shown in this work that decaying simulations without noise control always end up being noise dominated, since the system ends up with its gradients close to marginal and a flux approaching zero: the signal goes to zero with a finite noise. The absence of any temperature gradient evolution result in Ref. 29 makes a more detailed comparison with our simulations impossible.

C. ORB5 noise-controlled simulations

The simulations presented in Sec. III B have been run with the Krook operator with $\gamma_K = 9\times 10^{-5}$ Ω_i. This value corresponds to one-tenth of the maximal linear growth rate and should be small enough not to affect the heat transport.[21] The correction operator S_{corr} is such that no thermal energy is introduced in the system and the profiles will relax. These simulations will be called *noise controlled*.

By looking at the signal to noise ratio (Fig. 9), one clearly sees the beneficial influence of the noise control. When 80 m markers are used, the signal to noise ratio stays above 10 until $t\cong 8\times 10^4$ Ω_i^{-1}, twice longer as the transient
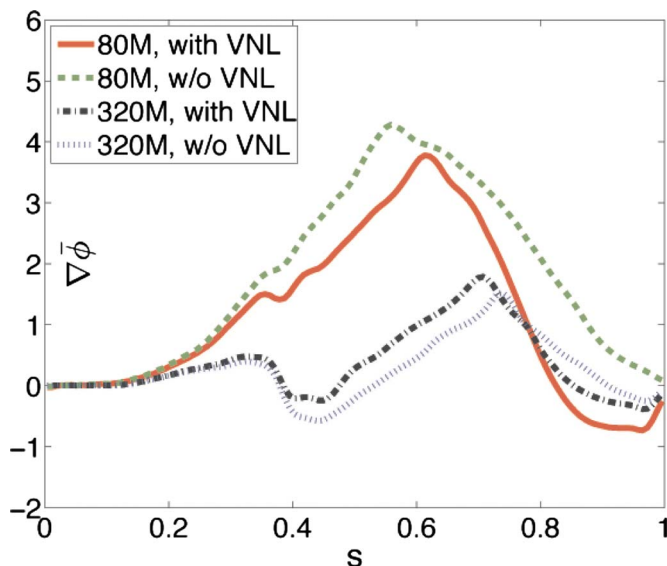
FIG. 10. (Color online) Profile of the radial electric field for noise-controlled simulations with 80 and 320 m markers, with and without the VNL. All profiles are time averaged between $t=2\times10^5$ and $t=2.5\times10^5$ Ω_i^{-1}.

FIG. 11. (Color online) χ_i/χ_{GB} as a function of R_0/L_{Ti} (both profiles are radially averaged between $\tilde{\rho}=0.4$ and $\tilde{\rho}=0.6$) for noise-controlled simulations with 80 and 320 m markers, with and without the VNL.

simulation. However, in decaying turbulence the signal rapidly becomes low and so the simulation becomes noisy. Nonetheless, a noise-controlled simulation with 320 m markers gives a rather satisfactory signal to noise ratio. Figure 10 displays profiles of the time-averaged radial electric field $\nabla\bar{\phi}$ for noise-controlled simulations with 80 and 320 m markers, with and without the VNL. Its effect is weak. With 80 m markers, the radial electric field has again a reversed sign at the edge when the VNL is turned off, but the profiles look relatively similar. When 320 m markers are used, the differences become even weaker and there is no spurious growth of the zonal flow near the edge. The most striking results of these simulations is the different zonal flow structures between the 80 and the 320 m cases. The 80 m noise-controlled case is still noisy. The noise accumulated in the axisymmetric $m=0$, $n=0$ zonal flow component is not Landau damped, so this component may grow indefinitely. It explains why the maximal value of the radial electric field is twice bigger in the 80 m case. In conclusion, one can argue that the irrelevance of the VNL on the zonal flow structure is necessary, but not sufficient condition for convergence.

Finally, the impact of the VNL on heat transport in noise-controlled simulations is examined on Fig. 11. Like for the transient cases, the 80 m noise-controlled fluxes rapidly become unphysical as the heat diffusivity stays constant while the gradient is continuously flattening. On the contrary, the 320 m noise-controlled fluxes look physical, as the final R_0/L_{Ti} is close to the nonlinear threshold of 6.[2] Note that the CYCLONE benchmark of ORB5 with the noise-control algorithm of Ref. [23] used 320 m markers. For this number, the simulations are converged and show that the VNL does not play any role in the heat transport.

In summary, these simulations reveal that although the noise issue is mostly discussed in the frame of electron temperatu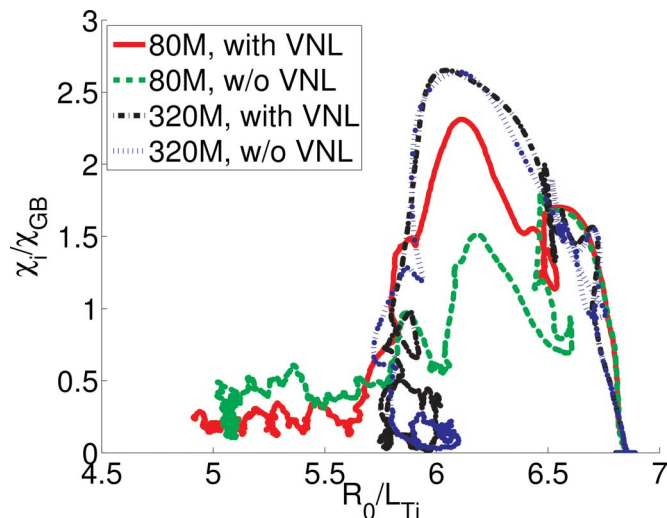re gradient turbulence,[20,30] it must not be neglected in ITG turbulence as well. The example of the VNL shows that noisy simulations may lead to a bad interpretation of physical effects. This is of course dangerous and it implies that PIC codes must be able to measure the noise in order to diagnose if the physical output of a simulation is reliable. In the particular case of ORB5, the simulations presented here clearly demonstrate the crucial role of the noise-control algorithm. According to the signal to noise criterion, the 320 m noise-controlled case can be run up to $t=1\times10^5$ Ω_i^{-1} before the signal to noise ratio falls below 10, which corresponds to 540 a/c_s. At this time, the noise level of this simulation is 20 times lower than the 320 m transient simulation, meaning that without artificial dissipation 6×10^9 of markers would be needed, which can be barely handled by present-day computers.

IV. SIMULATION RESULTS FOR DRIVEN TURBULENCE

In this section, the interesting case of driven turbulence is studied. As mentioned in Sec. II, the VNL may have a stronger case when the turbulence is not decaying. Therefore, *driven* CYCLONE ORB5 simulations with and without the VNL have been carried out by letting the Krook operator introduce thermal energy into the system. The gradients remain above the critical value and the signal can be kept high enough such that fewer markers are required as compared to the noise-controlled case. This is depicted on Fig. 12: 80 m markers are sufficient to keep the signal to noise ratio near 20.

Time-averaged profiles of radial electric field are shown on Fig. 13. The time average is in this case especially important due to the random burst activity. The profiles are very similar, showing again the weak influence of the VNL on the zonal flow profile. The only noticeable difference is at the edge. In fact, a significant difference has been observed on the zonal density, as can be seen on Fig. 14. A numerical buildup of charge appears in the nonlinear phase, whose sign
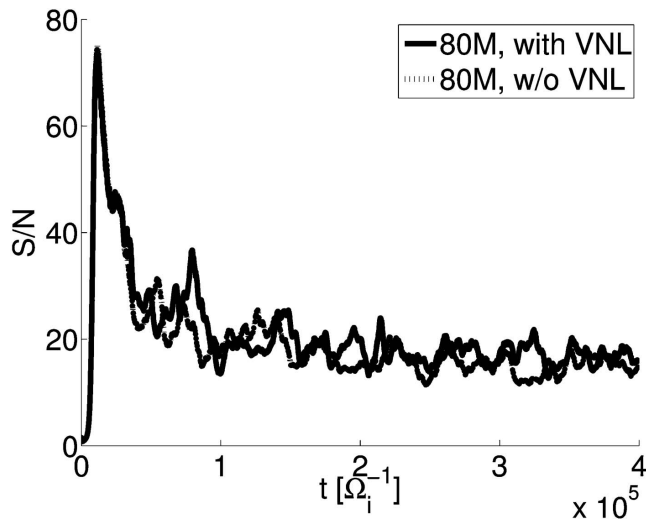
FIG. 12. Signal to noise ratio for driven simulations with 80 m markers, with and without the VNL. The horizontal dashed line indicates a signal to noise ratio of 10.

FIG. 14. Radial profile of the zonal density for 80 m driven simulations with and without the VNL, averaged between $t=1.5\times10^5$ and $t=2\times10^5$ Ω_i^{-1}.

differs depending on whether the VNL is retained or not. The quasineutrality equation is solved with the boundary condition $\phi=0$ at the plasma edge, which is imposed by setting $\delta n_i=0$ at the edge. However, markers near the edge have a nonzero weight, meaning that the quasineutrality is indeed violated in this region. This phenomenon is further enhanced as gyropoints lying outside the plasma are not taken into account in the charge assignment. This numerical density is then reflected in the zonal flow component $\phi^{(0,0)}$. This spurious zonal flow can be shielded by artificially increasing the equilibrium density in a narrow region near the edge. This scheme does not break the energy invariant of the model and has been first applied in the GT3D code.[31] It has been observed that this correction does not modify the fluxes and the profiles outside the shielding region.
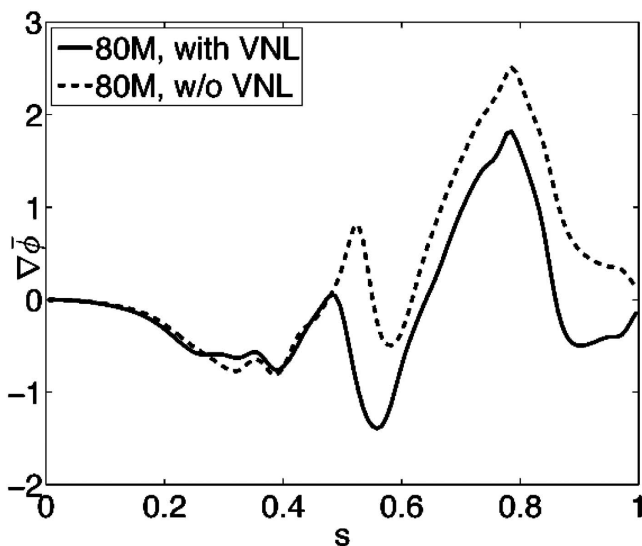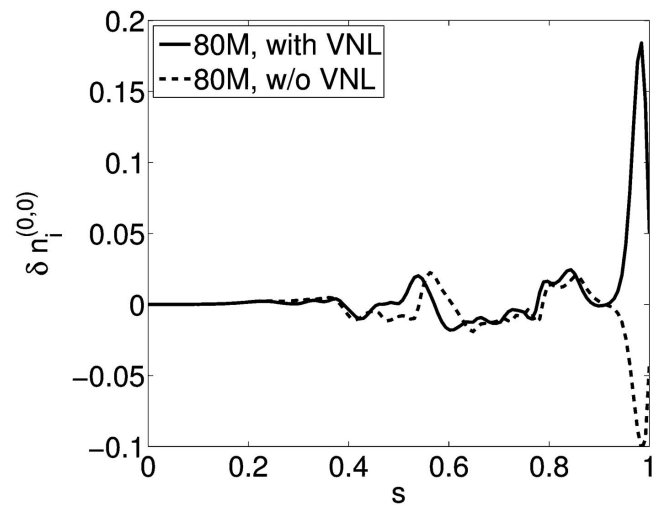

FIG. 13. Profile of the radial electric field for driven simulations with 80 m markers, with and without the VNL. All profiles are time averaged between $t=2\times10^5$ and $t=2.5\times10^5$ Ω_i^{-1}.

Up to now, the influence of the VNL on the heat diffusivity has been checked for decaying simulations, which are not really suited for quantitative predictions. On the other hand, driven simulations reach a steady state and are therefore able to quantify the heat transport. It is of course desirable to provide an error bar on the measured heat fluxes or heat diffusivities. For a given set of parameters, the error bar of a given quantity, say the heat diffusivity χ_i, is closely related to the intrinsic variability of the turbulence, which will be defined as the statistical variation of a physical quantity due to a change of initial conditions. Preferentially, a large number of simulations with different initial states but same physical and numerical parameters must be run to be able to make an ensemble average. This becomes especially important as the critical gradient is approached: the measured transport can have large relative variations. Consequently the variability of these simulations must be estimated as accurately as possible for both cases with and without the VNL. This is done as follows. For a given set of numerical and physical parameters, n_{sim} simulations are run with different initial states. The aim of these simulations is to measure a given physical quantity such as the ion diffusivity χ_i. For each individual simulation, a moving time average of χ_i, starting at time t_i and of width Δt_{ma}, is performed and will be written $\widetilde{\chi}_i$. The width Δt_{ma} must be large enough to include a typical life time of a burst. In this work, $\Delta t_{ma}=400a/c_s$ has been used, based on Ref. 32. Then, for each time, the average (respectively, the sample standard deviation) of $\widetilde{\chi}_i$ over the different simulations can be calculated, which will be written $\langle\widetilde{\chi}_i\rangle_n(t)$ [respectively, $s_n(\widetilde{\chi}_i)(t)$]. One distinguishes the sample standard deviation with the standard deviation (the difference is a factor $\sqrt{n_{\text{sim}}}/\sqrt{n_{\text{sim}}-1}$) as in practice $n_{\text{sim}}\gtrsim3$. The intrinsic variability of the heat diffusivity, noted V_{χ_i}, is then the average over time of $s_n(\widetilde{\chi}_i)(t)$,

$$V_{\chi_i}=\langle s_n(\widetilde{\chi}_i)\rangle_t.\tag{11}$$

The error bar of χ_i for a given set of physical parameters is chosen to be twice standard error of the mean, i.e.,
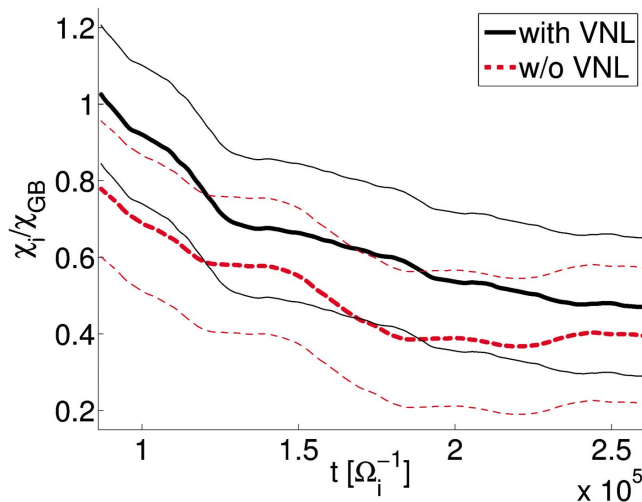
FIG. 15. (Color online) $\langle\tilde{\chi}_i\rangle_n(t)$ for the driven simulations at an initial $R_0/L_{Ti}=6.9$ with (black, solid line) and without (red, dashed line) the VNL. The thin lines are $\langle\tilde{\chi}_i\rangle_n(t)\pm 2I_{\chi_i}$ and represent the error bars of the simulations.

FIG. 17. (Color online) $\langle\tilde{\chi}_i\rangle_n(t)$ for the driven simulations at an initial $R_0/L_{Ti}=7.6$ with (black, solid line) and without (red, dashed line) the VNL. The thin lines are $\langle\tilde{\chi}_i\rangle_n(t)\pm 2I_{\chi_i}$ and represent the error bars of the simulations.

$2I_{\chi_i}=2V_{\chi_i}/\sqrt{n_{sim}}$ in order to have a 95.45% confidence interval. The procedure to fix the error bars on the heat diffusivity assumes that the simulations are numerically converged. Here, the convergence is based on Ref. 21. The number of markers is sufficient as the signal to noise ratio is around 20. The Krook damping coefficient is one-tenth of the maximum linear growth rate and is small enough. The driven simulations have been run with three different initializations: a white noise initialization, a mode initialization (described at Sec. II) with $n_1=10$, $n_2=30$, $m_1=14$, and $m_2=42$, and another mode initialization with $n_1=15$, $n_2=25$, $m_1=21$, and $m_2=35$. They will be called initializations 1, 2, and 3.

First, it has been checked that the radial electric field profiles are not affected by the initial conditions. Then, the heat diffusivity and the temperature gradient of the six driven simulations are analyzed in Figs. 15 and 16, which show the
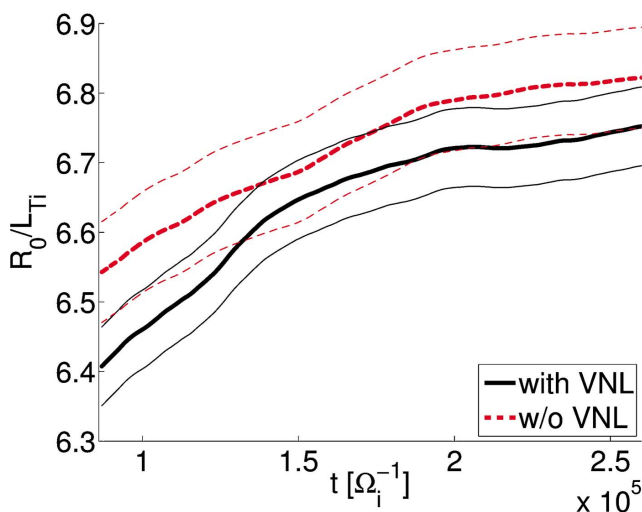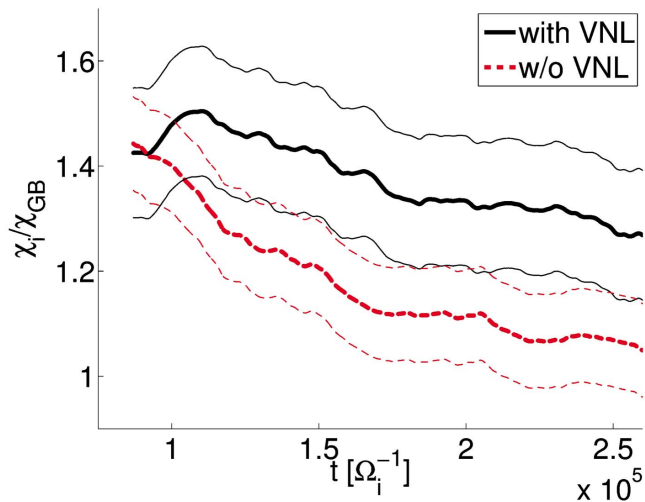
average of the moving time averages for the three simulations with and without the VNL with the corresponding error bars $2I_{\chi_i}$ and $2I_{R_0/L_{Ti}}$. The overlap between the two zones is large enough such that it can be argued that the VNL does not have a strong influence on the heat transport for the set of parameters considered here. Note however that the diffusivities are quite low because the temperature gradient is close to the marginal point. The same exercise has been repeated for CYCLONE simulations with higher initial gradients $R_0/L_{Ti}=7.6$.

The results of the six simulations are represented in Figs. 17 and 18. The two zones defined by $\langle\tilde{\chi}_i\rangle_n(t)\pm 2I_{\chi_i}$ and $\langle R_0/L_{Ti}\rangle_n(t)\pm 2I_{R_0/L_{Ti}}$ are barely overlapping. It means that for this set of parameters, the VNL has a small effect on the heat transport, all the more that the heat diffusivity is lower
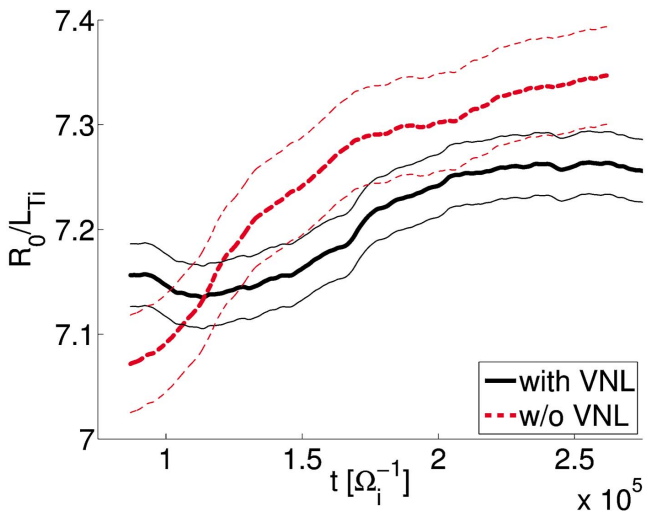

FIG. 16. (Color online) $\widetilde{\langle R_0/L_{Ti}\rangle}_n(t)$ for the driven simulations at an initial $R_0/L_{Ti}=6.9$ with (black, solid line) and without (red, dashed line) the VNL. The thin lines are $\langle\tilde{R}_0/L_{Ti}\rangle_n(t)\pm 2I_{R_0/L_{Ti}}$ and represent the error bars of the simulations.

FIG. 18. (Color online) $\widetilde{\langle R_0/L_{Ti}\rangle}_n(t)$ for the driven simulations at an initial $R_0/L_{Ti}=7.6$ with (black, solid line) and without (red, dashed line) the VNL. The thin lines are $\langle\tilde{R}_0/L_{Ti}\rangle_n(t)\pm 2I_{R_0/L_{Ti}}$ and represent the error bars of the simulations.
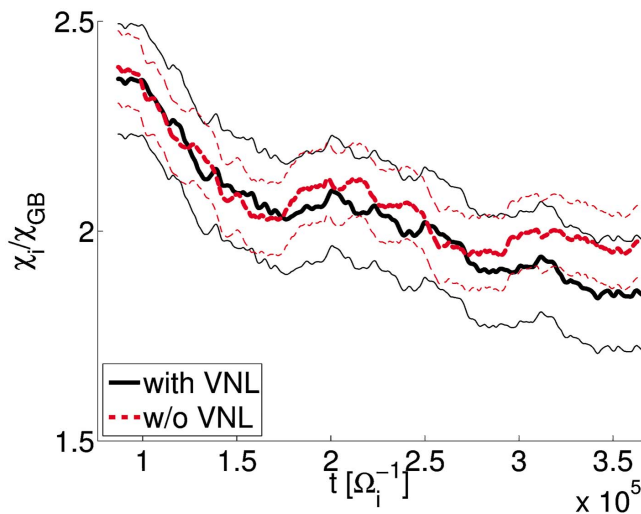
FIG. 19. (Color online) $\langle \tilde{\chi}_i \rangle_n(t)$ for the driven simulations at an initial R_0/L_{Ti}=8.4 with (black, solid line) and without (red, dashed line) the VNL. The thin lines are $\langle \tilde{\chi}_i \rangle_n(t) \pm 2I_{\chi_i}$ and represent the error bars of the simulations.

FIG. 20. (Color online) $\widetilde{\langle R_0/L_{Ti} \rangle}_n(t)$ for the driven simulations at an initial R_0/L_{Ti}=8.4 with (black, solid line) and without (red, dashed line) the VNL. The thin lines are $\langle \tilde{R}_0/L_{Ti} \rangle_n(t) \pm 2I_{R_0/L_{Ti}}$ and represent the error bars of the simulations.

while the temperature gradient is higher. This effect can nonetheless be considered as small because the two zones are disjointed but close. In order to check if this effect could be amplified, the same set of simulations with an initial gradient given by R_0/L_{Ti}=8.4 has been performed and the corresponding results are shown in Figs. 19 and 20. For these parameters the effect of the VNL on heat transport is almost negligible as the two zones are almost completely overlapping.

All these simulations show that the influence on the VNL on the radial electric field profile and on the heat transport in driven ITG simulations, if any, is small. This result is in agreement with the theoretical argument that the VNL is ρ^* smaller than the other terms. When the noise is controlled, driven simulations are easier to run as the signal to noise ratios are higher and remain constant. In fact, for driven turbulence the dissipation is also crucial for the decaying case. Driven simulations must be run longer to be able to make quantitative predictions. A reasonable simulation length would be around $800a/c_s$,[21,32] corresponding to $t \cong 1.5 \times 10^5 \; \Omega_i^{-1}$. In Ref. 21, simple estimations of signal to noise ratios are given. For a transient case the signal to noise ratio goes like $1/t_f$, where t_f is the final time of the simulation, while in the noise-controlled case it goes like γ_K. With $\gamma_K=9 \times 10^{-5}$, it means that a similar driven simulation without dissipation would require 13 times more markers than the one presented in this section. Even if these are only approximations, it means that standard collisionless PIC simulations at $\rho^* \sim 1/200$ need at least 1×10^9 of markers if they have to be run for meaningful times. In this respect, introducing artificial dissipation becomes almost mandatory. As an alternative to the noise-control algorithm, the coarse-graining method[33] is another possible solution. It is also possible to provide physical dissipation to the system by implementing a collision operator, but this task is extremely difficult to realize in a PIC code due to the weight-spreading phenomenon.[34] Possible solutions to solve this problem have been
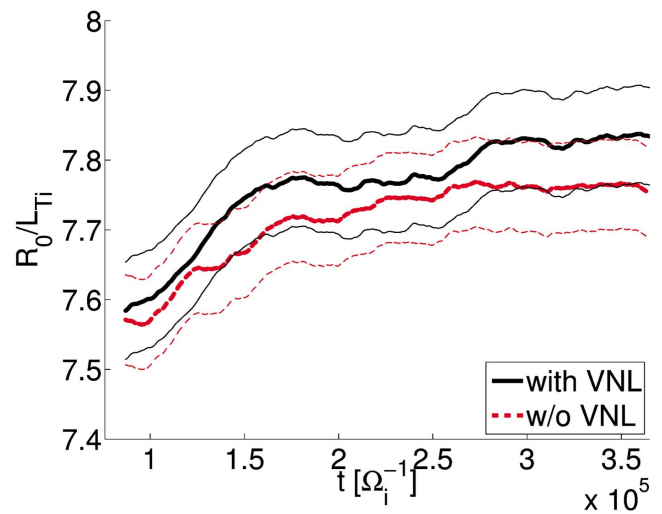
proposed[35,36] but have not been implemented in a five-dimensional PIC code yet.

All the results presented in this section dealt with heat transport. The same analysis could be carried out for parallel momentum transport. However, as mentioned in Sec. II, the Krook operator does not conserve parallel momentum. A more careful study must be done by enforcing the Krook operator to conserve the parallel momentum.

V. CONCLUSION

In this work, the role of the parallel nonlinearity in PIC ITG simulations has been carefully studied with the collisionless global PIC codes TORB and ORB5. The two problems of decaying and driven turbulence have been considered. The revisited TORB simulations have proven that an incorrect use of noise reduction techniques may lead to erroneous conclusions. In the case of decaying turbulence, the ORB5 results clearly show that the effect of the VNL on the zonal electric field is in fact an effect of the statistical noise. By increasing the number of markers and turning on the noise-control algorithm, converged simulations are obtained and the VNL does not affect the physical output anymore. Therefore, one of the most important outcomes of this paper is that the numerical noise issue, often neglected in ITG simulations, deserves careful attention as well. In particular, a simple estimation on the number of markers required to converge a collisionless, nondissipative ITG PIC simulation (driven or decaying) reveals that this number is huge and can barely be resolved in present day computers, meaning that some form of dissipation must be added into the system. This paper confirms the necessity for PIC codes to be able to measure numerical noise in order to avoid a bad interpretation of the results. This explanation should hopefully put an end to the controversy that occurred on the role of the VNL. In addition, its effect on heat transport in ITG driven

simulations has been studied for the first time, and the conclusion is that this effect, if any, is small. Finally, note that this conclusion only applies for heat transport in ITG simulations. No statement on particle transport or trapped electron mode turbulence can be inferred from this work. Also, the presence of collisions might modify the present conclusions. All these topics are left for future studies.

ACKNOWLEDGMENTS

[1] X. Garbet, Plasma Phys. Controlled Fusion **43**, A251 (2001).

[2] A. M. Dimits, G. Bateman, M. A. Beer, B. I. Cohen, W. Dorland, G. W. Hammett, C. Kim, J. E. Kinsey, M. Kotschenreuter, A. H. Kritz, L. L. Lao, J. Mandrekas, W. M. Nevins, S. E. Parker, A. J. Redd, D. E. Shumaker, R. D. Sydora, and J. Weiland, Phys. Plasmas **7**, 969 (2000).

[3] J. B. Taylor and R. J. Hastie, Plasma Phys. **10**, 479 (1968).

[4] P. H. Rutherford and E. A. Frieman, Phys. Fluids **11**, 569 (1968).

[5] E. A. Frieman and L. Chen, Phys. Fluids **25**, 502 (1982).

[6] W. W. Lee, Phys. Fluids **26**, 256 (1983).

[7] D. H. E. Dubin, J. A. Krommes, C. Oberman, and W. W. Lee, Phys. Fluids **26**, 3524 (1983).

[8] R. G. Littlejohn, J. Plasma Phys. **29**, 111 (1983).

[9] T. Hahm, Phys. Fluids **31**, 2670 (1988).

[10] T. S. Hahm, Phys. Plasmas **3**, 4658 (1996).

[11] A. J. Brizard, J. Plasma Phys. **41**, 541 (1989).

[12] B. H. Fong and T. S. Hahm, Phys. Plasmas **6**, 188 (1999).

[13] J. Candy, R. E. Waltz, S. E. Parker, and Y. Chen, Phys. Plasmas **13**, 074501 (2006).

[14] L. Villard, P. Angelino, A. Bottino, S. J. Allfrey, R. Hatzky, Y. Idomura, O. Sauter, and T. M. Tran, Plasma Phys. Controlled Fusion **46**, B51 (2004).

[15] J. C. Kniep, J. N. G. Leboeuf, and V. C. Decyck, Comput. Phys. Commun. **164**, 98 (2004).

[16] L. Villard, S. J. Allfrey, A. Bottino, M. Brunetti, G. L. Falchetto, V. Grandgirard, R. Hatzky, J. Nührenberg, A. G. Peeters, O. Sauter, S. Sorge, and J. Vaclavik, Nucl. Fusion **44**, 172 (2004).

[17] Y. Idomura, M. Ida, S. Tokuda, and L. Villard, J. Comput. Phys. **226**, 244 (2007).

[18] R. Hatzky, T. M. Tran, A. Könies, R. Kleiber, and S. J. Allfrey, Phys. Plasmas **9**, 898 (2002).

[19] S. Jolliet, A. Bottino, P. Angelino, R. Hatzky, T. M. Tran, B. F. McMillan, O. Sauter, K. Appert, Y. Idomura, and L. Villard, Comput. Phys. Commun. **177**, 409 (2007).

[20] A. Bottino, A. G. Peeters, R. Hatzky, S. Jolliet, B. F. McMillan, T. M. Tran, and L. Villard, Phys. Plasmas **14**, 010701 (2007).

[21] B. F. McMillan, S. Jolliet, T. M. Tran, L. Villard, A. Bottino, and P. Angelino, Phys. Plasmas **15**, 052308 (2008).

[22] P. Angelino, A. Bottino, R. Hatzky, S. Jolliet, O. Sauter, T. M. Tran, and L. Villard, Phys. Plasmas **13**, 052304 (2006).

[23] G. L. Falchetto, B. D. Scott, P. Angelino, A. Bottino, T. Dannert, V. Grandgirard, S. Janhunen, F. Jenko, S. Jolliet, A. Kendl, B. F. McMillan, V. Naulin, A. H. Nielsen, M. Ottaviani, A. G. Peeters, M. J. Pueschel, D. Reiser, T. Ribeiro, and M. Romanelli, Plasma Phys. Controlled Fusion **50**, 124015 (2008).

[24] A. Y. Aydemir, Phys. Plasmas **1**, 822 (1994).

[25] E. Rafajlowicz and R. Schwabe, Stat. Probab. Lett. **76**, 803 (2006).

[26] J. A. Krommes, Phys. Plasmas **6**, 1477 (1999).

[27] P. H. Diamond, S. I. Itoh, K. Itoh, and T. Hahm, Plasma Phys. Controlled Fusion **47**, R35 (2005).

[28] A. Bottino, Ph.D. thesis, Ecole Polytechnique Federale de Lausanne, 2004.

[29] W. W. Lee, S. Ethier, R. Kolesnikov, W. X. Wang, and W. M. Tang, Computational Science and Discovery **1**, 015010 (2008).

[30] W. M. Nevins, G. W. Hammett, A. M. Dimits, W. Dorland, and D. E. Shumaker, Phys. Plasmas **12**, 122305 (2005).

[31] Y. Idomura (private communication).

[32] J. Candy, R. Waltz, and W. Dorland, Phys. Plasmas **11**, L25 (2004).

[33] Y. Chen and S. E. Parker, Phys. Plasmas **14**, 082301 (2007).

[34] Y. Chen and R. B. White, Phys. Plasmas **4**, 3591 (1997).

[35] S. Brunner, E. Valeo, and J. A. Krommes, Phys. Plasmas **6**, 4504 (1999).

[36] J. L. V. Lewandowski, Phys. Plasmas **12**, 052322 (2005).